

# Design and Experimental Analysis of a DC to 1MHz Closed Loop Magneto-resistive Current Sensor

G. Laimer and J. W. Kolar

Swiss Federal Institute of Technology (ETH) Zurich  
Power Electronic Systems Laboratory  
ETH Zentrum, ETL/H17  
CH-8092 Zurich, Switzerland, Europe

Tel.: +41-1-632-7447

Tel.: +41-1-632-2834

email: laimer@lem.ee.ethz.ch

email: kolar@lem.ee.ethz.ch

**Abstract** - This paper presents the improvement of a commercially available current sensor based on the anisotropic magneto-resistive effect for applications requiring high bandwidth current measurement such as high switching frequency single-phase and three-phase unity power factor PWM rectifier systems. The sensor concept is of special interest as it could be packaged into compact power processing units and integrated power electronic modules. In this paper the anisotropic magneto-resistive effect, as well as the analog interface electronic for signal conditioning for integrated current sensing are discussed. The sensor functional principle, the advantages and limitations are shown in detail. The measured sensor characteristics are also shown. Finally, improvements are discussed which involves further reduction of the size and the offset calibration procedure.

## I. INTRODUCTION

As next generation of power processing units will be operate at ultra high switching frequencies in order to achieve a high power density, high bandwidth, noise-immune current sensors will be required. Hall effect-based current sensors, both open- and closed-loop are widely used in power electronics systems. These sensors provide galvanic isolation and DC to 250kHz AC operation, but show a number of disadvantages. Due to the low sensitivity the sensor relies on a magnetic core for concentrating the magnetic flux around the current carrying conductor, which makes the sensors bulky and not suitable for integration. Furthermore, Hall effect-based sensors also have limitations concerning linearity, temperature stability and temperature range of operation.

In contrast, anisotropic magneto-resistive (AMR) current sensors which are commercially available since several years [1-3], are highly attractive for integration into power electronics systems and modules. However, the application area of such sensors is still limited by a low bandwidth of 100kHz [4], although a frequency limit of about 1MHz is stated in [5] with reference to the physical properties of the magneto-resistive (MR) sensing element. This leads to the assumption that the frequency performance of the current sensor can be extended significantly.

In this paper, the AMR effect is described in **Section 2**. The utilization of the AMR sensor physical properties in current sensing applications is discussed. In **Section 3** the principle of operation, the signal conditioning electronics and the method for compensating the offset and temperature drift are described. A solution for improving the frequency performance is then given. Based on this solution, the experimental results are shown and discussed in **Section 4**. These experiments include measuring the frequency response, current

sensing linearity and the noise immunity performance of the wide bandwidth current sensor. Finally in **Section 5** improvements for integrating the sensor signal conditioning electronic into an ASIC are mentioned as well as the utilization of the AMR device as a temperature monitor. Furthermore, future fields of applications are highlighted.

## II. ANISOTROPIC MAGNETO-RESISTIVE EFFECT (AMR) – PHYSICAL PROPERTIES

The anisotropic magneto-resistive effect is seen as a change of the resistance of ferromagnetic materials for changing magnetic field. An AMR sensor is composed of a nickel iron alloy (permalloy  $Ni_{81}Fe_{19}$ ) structure manufactured with a thin film technique. These sensing elements have a strip shaped (narrow and stretched) geometry with a thickness of approx. 30nm. For this structure, resistor values with sufficient accuracy and sensitivity can be realized. Due to the manufacturing process this ferromagnetic strip shows a distinct inner magnetic field  $M_0$  (magnetic dipole) along the x-direction (cf. **Fig.1**). If a current  $I$  is impressed along the x-axis, the current and the resulting magnetic field  $M=M_0$  are in parallel ( $\theta=0^\circ$ ). In this case the strip has the maximum resistance  $R_0$ . When exposing the sensor to an external magnetic field  $H_y$  in the sensitivity axis (y-direction) the resulting magnetic field  $M=M_0+H_y$  will be rotated out of the x-axis by an angle of  $\theta$ , and the resulting resistance can be calculated ((1) in [4]) as:

$$R(\Theta) = R_0 - \Delta R \sin^2(\Theta) . \quad (1)$$

Since the AMR devices change their resistance with the square of the magnetic field, they are not sensitive to the applied external magnetic field direction. Other disadvantages include a small variation in resistance ( $\Delta R_{max} < 3\%$ ), a strong non-linearity and a distinct temperature characteristic ( $0.3\%/^\circ K$ ). A temperature variation of  $10^\circ C$  takes larger influence on the resistance of the AMR than could be achieved at maximum by an external magnetic field. Therefore, the realization of a high performance current transducer is not possible for employing only a single permalloy-strip. The non-directionality of the single permalloy-strip can be corrected by “barberpole biasing”. This is named from the pattern formed by aluminum shorting bars across the width of the permalloy-strip, made by a vaporization process, at a  $45^\circ$  angle (cf. **Fig.2(a)**). The aluminum thin film shorting bars form (approximately) equipotential lines and the impressed current  $I$  flows from one bar to the following, taking the shortest path through the permalloy-strip, along a  $-45^\circ$  angle. Altering the direction of the current through the device at a  $-45^\circ$  angle shifts the operating point down by a value of  $-\Delta R/2$  (cf. **Fig.2(b)**).

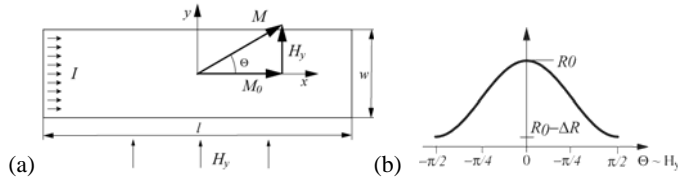


**Fig.1:** (a) Ferromagnetic  $Ni_{81}Fe_{19}$  permalloy strip with length  $l$ , width  $w$  and thickness  $t$ . The strip shows a distinct inner magnetization  $M_0$  along  $x$ -direction. When exposing the permalloy strip to an external magnetic field  $H_y$  (the axis of sensitivity is the  $y$ -axis) the resistance  $R(\theta)$  decreases dependent on the strength of the magnetic field. (b) The change in resistance depends on the square of the magnetic field. Therefore, this sensor-element is not sensitive on the magnetic field polarity.

Now the sensor element is sensitive to the polarity of magnetic fields. If the device is manufactured with opposite-direction barberpoles ( $-45^\circ$ ) the characteristic is mirrored along the  $y$ -axis, as shown by the dashed line in Fig.2(b). When exposing the sensor elements (one element with  $45^\circ$  and the other element with  $-45^\circ$  barberpoles) to the same magnetic field  $H_y$ , the resistance of one sensor element changes by  $+R$  and the resistance of the other sensor element changes by  $-R$ .

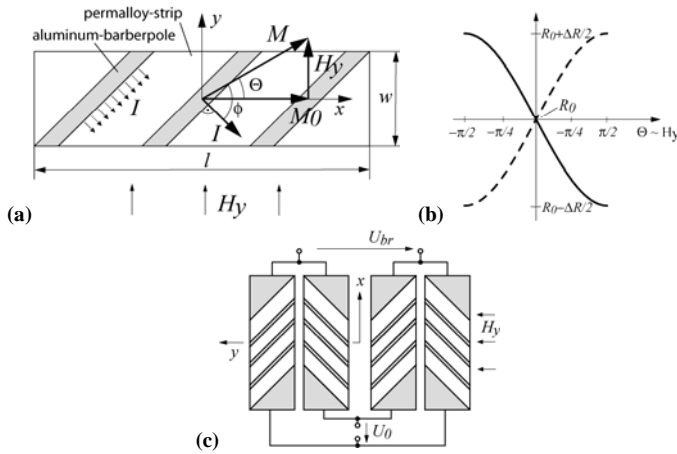


**Fig.2:** (a) Permalloy-strip with barberpole biasing. (b) When exposing a sensor device (with  $45^\circ$  barberpole biasing) to a magnetic field  $H > 0$  the resistance of the magneto-resistor is reduced. A magnetic field  $H < 0$  increases the resistance value. The dashed line shows an inverse behavior of the sensing element, given with a  $-45^\circ$  barberpole structure. With  $H_y = 0$  the magneto-resistor shows in both cases a value of  $R_0$ . (c) Four barberpole sensing devices are combined to a Wheatstone bridge arrangement in order to increase the sensitivity and reduce the temperature drift of the bridge output voltage.

A combination of four individual sensor devices in a Wheatstone bridge arrangement (cf. Fig.2(c)) increases the sensitivity and limits the effect of the large temperature dependency. The output signal can be maximized by arranging the sensor devices such that the output of one bridge leg increases while the output of the other bridge leg decreases, what doubles the bridge sensitivity. There, the sensors must be matched in sensitivity and temperature dependency in order to take full advantage of the bridge topology.

Due to the high conductivity of the barberpole strips, the active AMR area of the strip is reduced and therefore the sensor's sensitivity is lowered. An additional negative effect of using barberpole biasing is the potential to change the sensors magnetization if the device is exposed to a high magnetic field in ( $-x$ )-direction (inverse to the direction of  $M_0$ ). In this case the direction of the device's magnetization can switch, which inverts the slope of the resistance

change with respect to the magnetic field. Therefore, permanent magnets are placed close to the sensor element in a way that the magnetization  $M_0$  will be increased in the  $x$ -direction ( $M_0' = M_0 + M_{bias}$ ), what reduces the likelihood of a switch in magnetization significantly, but lowers the sensitivity of the sensor.

### III. CURRENT SENSOR BASED ON THE AMR EFFECT

In this section, the principle of operation of the AMR sensor is described briefly. A block diagram is given in order to discuss the sensor bandwidth limit. The single elements of the block diagram are identified in gain and frequency response. Furthermore, the need for compensating the sensor offset and temperature drift is discussed.

#### A. Principle of Operation

Although improvements in linearity can be achieved by the barberpole structure, the nonlinearity is still very high and thus a compensation technique is applied for current sensing (cf. Fig.3(a)). There, an aluminum compensation conductor is placed in close vicinity above the AMR-sensor device and separated by a  $SiO_2$  isolation layer (cf. Fig.3(b)). The Wheatstone bridge, composed of the MR barberpole devices, is connected to the input of an operational amplifier [1], which drives a push-pull output stage. This output stage generates the compensating current  $i_{comp}$ , producing a compensating magnetic field  $H_{comp}$  to null the magnetic field  $H_{prim}$ , produced by the current  $I_{prim}$  in the current-carrying conductor. With a resistor  $R_s$  the compensating current is converted into a voltage  $U_a$ , which is related to the current to be measured. The sensor operates with a bridge output voltage near zero and therefore the sensor nonlinearity is minimized. Since the magnetic fields strength changes in inverse proportion to the distance, precise positioning is required with respect to the current-carrying (primary) conductor.

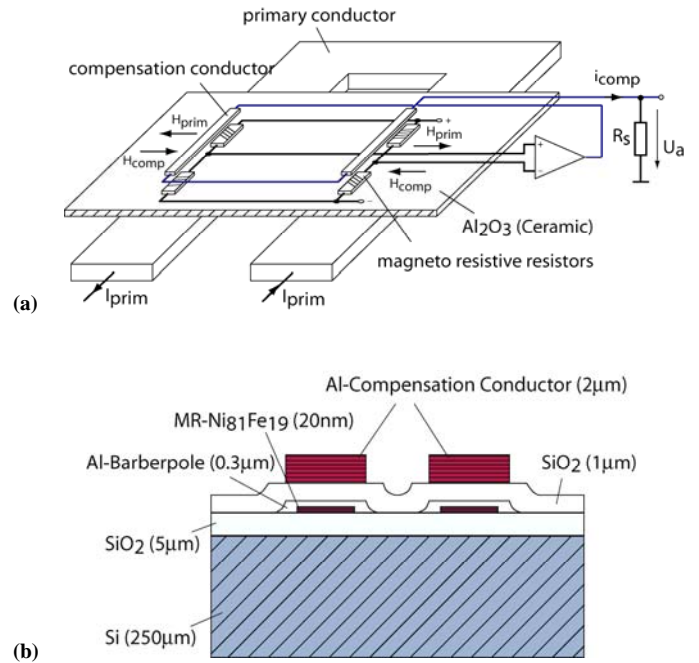


**Fig.3:** (a) AMR-sensors in Wheatstone bridge arrangement. The bridge output is connected to the input of an op-amp, which drives the compensating current  $i_{comp}$ . A resistor  $R_s$  converts the compensating current into a voltage which is proportional to the current to be measured. (b) Cross-section of the AMR-sensor device. The magneto-resistive permalloy-strip with barberpole structure is mounted on a silicon plate.

## B. Control-Oriented Block Diagram

The control-oriented block diagram (cf. Fig.4(a)) of the sensor, was determined by a series of measurements. First, the resulting bridge output voltage  $\Delta U_{br}$  was measured for an impressed low-frequency primary current  $i_1$  with the compensation loop disconnected ( $i_{comp}=0$ ) resulting in a sensor gain of  $\Delta U_{br}/i_1=K \cdot S_1=0.5 \cdot 10^{-3} V/A$ . A second measurement provides the gain of the compensation-loop as  $\Delta U_{br}/i_{comp}=K \cdot S_1=0.5 V/A$ . The ratio of the secondary and primary gain is  $K \cdot S_2/K \cdot S_1=1000$ . In order to remain in the linear range of the sensors characteristic  $\Delta U_{br}(\Delta H_y)$  all measurements were made with small signal excitation.

A measured small-signal frequency response of the nonlinear sensor characteristic  $S_2K$  is depicted in Fig.8, and shows the limited performance of the AMR-sensor element at high frequencies. In order to show only the principle sensor behavior in the following calculations it is assumed that  $S_1K$  is proportional to  $S_2K$ , and frequency-independent.

The open-loop gain  $v_g$  of the op-amp (TLE2037) is given in the datasheet [7] and can be approximated as

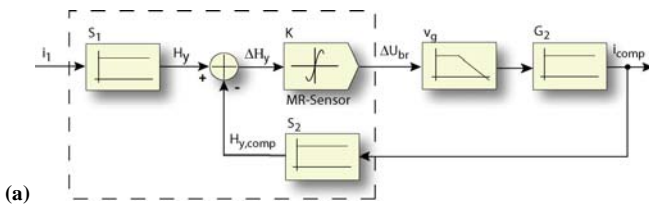
$$v_g(s) = k_0 \frac{1}{1+sT_1} \frac{1}{1+sT_2} \quad (3)$$

The parameters of the given op-amp are:  $k_0=155dB$ ,  $T_1=0.16s$ ,  $T_2=6.18 \cdot 10^{-9}s$ .

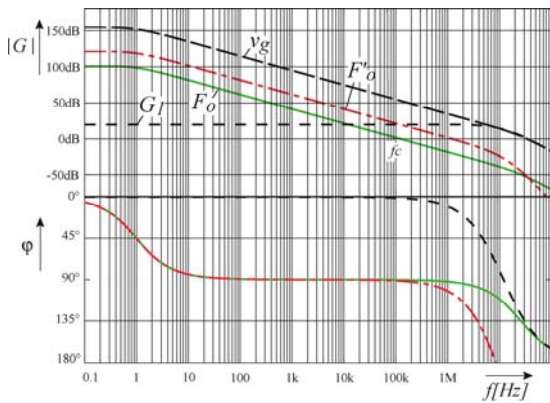
The open-loop transfer-function of the sensor can be expressed as

$$F_o(s) = S_1K \cdot v_g \cdot G_2 \cdot 1000 \quad (4)$$

The factor  $G_2=1/230\Omega$  converts the output voltage of the op-amp into the compensating current  $i_{comp}$ . The factor  $1/G_2$  represents the resulting DC resistance of the series connection of the compensation conductor  $R_{comp}$  and the resistor  $R_c$  (cf. Fig.3(a)), as seen by the output of the op-amp when driving the compensating current.



(a)



(b)

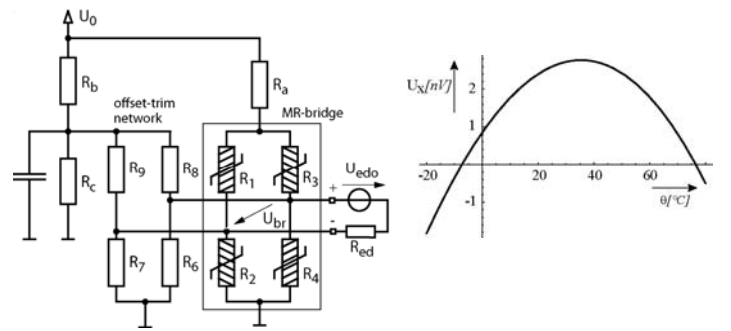
**Fig.4:** (a) Control-oriented block diagram of the current sensor. The elements of the block diagram encircled by a dashed line are determined by the sensors physical behavior. An op-amp, in open-loop operation, amplifies the output of the Wheatstone bridge  $\Delta U_{br}$  and drives a compensating current to null the magnetic field  $\Delta H_y$ . (b) Bode-Plot of the frequency dependency of the op-amp open loop gain  $v_g$ ; resulting current sensor open-loop frequency response  $F_o$ , additional amplifier gain  $G$ ; improved frequency response  $F'_o$ .

An analysis of the sensors open-loop behavior in Eq.(4) reveals that although an op-amp with a unity-gain bandwidth product of  $f_{GBWP}=25MHz$  is employed, the sensor's frequency bandwidth is limited to  $f_c \approx 100kHz$ . Therefore, the frequency performance of the AMR effect (c.f. Fig.8) is not fully utilized. This is because the loop-gain in the forward path  $F_o(s)$  is reduced by  $S_1K \cdot G_2 \cdot 1000 = -53dB$ , resulting in a crossover frequency of  $f_c=100kHz$  (cf. Fig.4(b)). For frequencies higher than the crossover frequency the op-amp is not able to null the magnetic field of the current carrying conductor. An improvement in bandwidth can be easily achieved by inserting an additional amplifier stage, with a gain of  $G_I=20 \dots 25dB$ , at the output of  $v_g$ , as indicated with the dashed line in Fig.4(b). This results in a significantly increased crossover frequency  $F'_o(s)=0dB$  of about 1MHz. The same result can be achieved by selecting a single op-amp with a sufficiently large unity-gain bandwidth product.

## C. Offset Trim and Temperature Drift Compensation

Magneto-resistive materials exhibit a significant temperature dependency. The temperature dependency of each magneto-resistor of the bridge ( $R_1 \dots R_4$ ) was measured within a small temperature range of  $[20^\circ C \dots 60^\circ C]$ . Using curve fitting techniques to the measured data points a linear temperature coefficient (for the small temperature range) of  $\alpha = 2.13 \cdot 10^{-3} 1/^\circ K$  for each resistor was obtained. Due to the manufacturing tolerances the resistor values do not ideally match what results in an offset-voltage  $U_{br}$  being present for zero primary current. Assuming an equal temperature coefficient of all resistors in the AMR-bridge experience the same change in resistance for changing temperature, and therefore a temperature variation does not affect the offset-voltage. The offset-voltage has to be compensated in order to avoid an offset of the current sensing. A trim-network for compensating the offset-voltage is shown in Fig.5(a). Unfortunately, the bridge output voltage now becomes temperature dependent in conjunction with the trim-network. The compensation network in parallel with the AMR-bridge has to compensate the offset due to the manufacturing tolerances of the sensor device and also the offset of the adjacent op-amp stage  $U_{edo}$ . Furthermore, the compensation network has to ensure a low variation of the bridge output voltage with temperature.

In the following, a procedure for determining the resistors  $R_7 \dots R_9$  and  $R_c$  of the compensation network for the laboratory sensor setup will be discussed. The procedure was implemented in a *Mathematica* script.



(a)

(b)

**Fig.5:** (a) Offset trim and temperature compensation network in parallel to the Wheatstone bridge.  $U_{edo}$  and  $R_{ed}$  denote the op-amp offset voltage and differential input resistance respectively. (b) Temperature dependency of the AMR Wheatstone bridge with optimized trim network. For employing the optimized trim-network only a small output voltage (in the range of nV) is remaining (cf (7)).

The supply voltage  $U_0$ , the values of the resistors  $R_1 \dots R_4$  (at  $20^\circ\text{C}$ ) and the temperature coefficient  $\alpha$  of the Wheatstone bridge resistors are measured, as well as the resistor  $R_a$ , and are considered as given parameters. The initial resistance values  $X_i = [R_6, R_7, R_8, R_9, R_a, R_b]$  are selected by a random number generator in a predefined range:  $X_{i,init} = \text{Rand}\{X_i\}$ . The target is to find a combination of values for the resistors  $X_i$  in order to get a bridge output voltage which compensates the op-amp offset voltage, i.e.  $u_x = U_{br} - U_{edo} \rightarrow 0$ , for a given temperature range. With the initial values  $X_{i,init}$ , the Integral of Squared Error (ISE) of  $u_x$  is calculated

$$ISE = \int_{\Theta=-20^\circ\text{C}}^{80^\circ\text{C}} (U_{br}(X_i) - U_{edo})^2 d\Theta \rightarrow \min \quad (5)$$

and minimized by parameter variation. This calculation will be done cyclically (approx. 100 times) keeping the values for the optimal solution  $X_{i,opt}$ . A plot of  $u_x$  versus the temperature is given in Fig.5(b). It turns out that the accuracy of the calculated resistors  $X_{i,opt}$  has to be higher than 0.1% in order to limit  $u_x(\Theta)$  to a sufficiently small value for a given temperature range.

For deriving an estimation of the admissible error voltage  $u_x$  for a sensor accuracy higher than 0.1% one has to consider that an error voltage  $u_x \neq 0$  is amplified by the open-loop gain of the op-amp  $v_g$ , which in turn produces a compensating current  $i_k$  through the compensation conductor  $R_{comp}$  and the resistor  $R_s$  (cf. Fig.3(a)). This compensation current results an AMR-bridge output voltage forcing the voltage across the op-amp differential resistor  $R_{ed}$  to zero. This closed-loop behavior is described by the relation

$$\frac{i_k}{u_x} = \frac{v_g}{S_2 v_g + (R_s + R_{comp})} \cong \frac{1}{S_2} \quad (6)$$

There, the factor  $(R_s + R_{comp})/v_g \ll 1$  can be neglected due to the high gain of the op-amp stage. The output signal of the sensor, measured across the resistor  $R_s$ , is  $U_a = \pm 2.5V$  at the nominal primary current  $\pm I_{pm}$ . Therefore, the compensation current at nominal input current is  $i_{comp} = I_{pm}/1000 = 25mA$  (for the CMS2025 type). For an admissible deviation of  $< 0.1\%$  the error voltage has to remain below

$$u_x < i_{comp} S_2 = 0.0001 \cdot 25mA \cdot 0.5A/V = 12.5\mu V \quad (7)$$

In practice, the resistors of the compensation network have to be laser-trimmed during a compensation procedure in order to bring the offset voltage to zero.

#### IV. EXPERIMENTAL RESULTS

The modified sensor (cf Fig.9) is tested with a single-phase boost converter operating at a switching frequency of  $f=500kHz$ . A 100MHz TEK current probe (TEK A6302) was used as a reference to evaluate the frequency performance of the investigated current sensors. Two concepts for improving the bandwidth are tested. One concept (MR-Sensor 1) is to employ one op-amp with a large unity-gain bandwidth product ( $GBP=80MHz$ ). The other concept (MR-Sensor 2) is a series connection of two amplifier stages with the same type of op-amp also having a  $GBP$  of 80MHz. In this case one op-amp is operating in open-loop mode and the second op-amp stage is realizing an inverting amplifier stage with a gain of  $G_1=8.5dB$ . The intention of MR-Sensor 1 was to simply replace the op-amp in the commercial sensor by a higher bandwidth device. The output signal of the modified sensor shows a good match with the reference signal (cf Fig.6, MR-Sensor 1). It can be seen that the edges of the triangular signal are smoothed in comparison with the reference signal. This is because of the decreasing loop-gain for higher frequencies. In order to further

improve the frequency performance of the sensor an op-amp with higher unity-gain bandwidth product could be used.

Unfortunately, op-amps with increasing frequency performance show a larger offset voltage and higher offset voltage drift and result in higher sensor realization costs. Therefore, the concept of MR-Sensor 2 is applied in order to further increase the loop-gain for high frequency components of the signal to be measured, despite using op-amps with medium frequency performance.

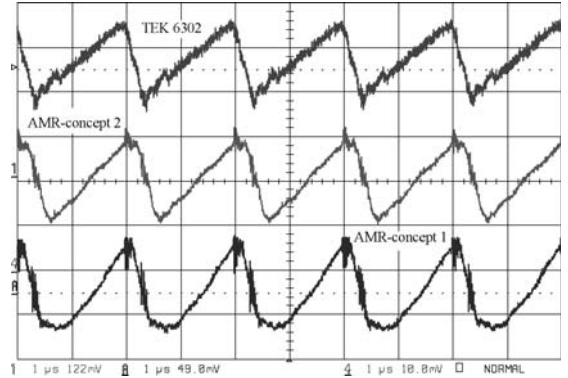


Fig.6: Measured results of the modified commercial AMR-current sensor. The signal labelled with *AMR-concept 1* corresponds to the concept with a single op-amp, whereas the signal labelled with *AMR-concept 2* corresponds to the concept with two amplifier stages connected in series.

The measurement results show an excellent dynamic performance (cf. Fig.6, MR sensor 2). Only, a small deviation in shape and a small phase shift are present compared to the reference signal measured with a 100MHz TEK 6302 current probe (cf. Fig.7). This is mainly caused by the limited bandwidth of the sensing element (cf Fig.8).

*Remark:* In order to increase the gain of the op-amp for high frequencies one could use a lead element instead of using a large bandwidth op-amp. The lead element shows an increasing gain of 20dB/dec up to a limited frequency. The limit is given by open-loop gain of the op-amp, which decreases over frequency with -20dB/dec. At the frequency limit, where the gain of the lead element reaches the open-loop gain of the op-amp, the gain changes from +20dB/dec to -20dB/dec. This change in gain by 40dB/dec is associated with a large phase shift and reduces the phase margin for high frequency components and in turn leads to instability of the amplifier stage and/or results in a large output signal ringing when the input signal is changing its slope. Therefore, a lead element could not be employed for increasing the gain for higher frequencies in the case at hand.

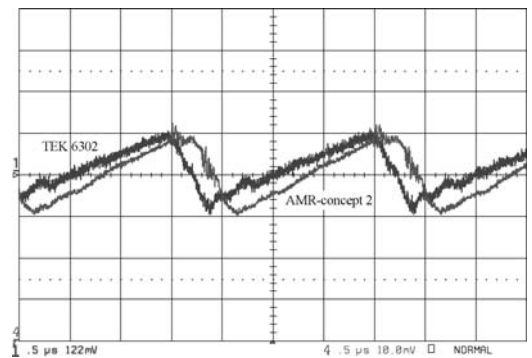


Fig.7: The AMR-sensor output signal (*AMR-Sensor 2*) shows a small deviation in the signal shape and a phase shift in comparison to the reference signal, measured with the TEK 6302 current probe.

According to Fig.7 the sensor shows a high  $dv/dt$ -immunity as the high rate of change of the boost converter drain source voltage ( $20kV/\mu s$ ) does result only in a negligible distortion of the sensor output signal.

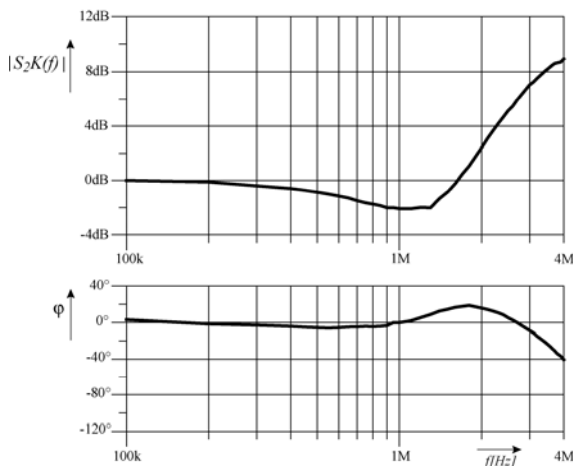


Fig.8: The measured normalized frequency response  $\Delta U_{br}/\hat{i}_{comp}=S_2K(f)$  of the compensation path shows a roll off in gain at 100kHz. At 1MHz the gain is reduced by a factor of -2dB.

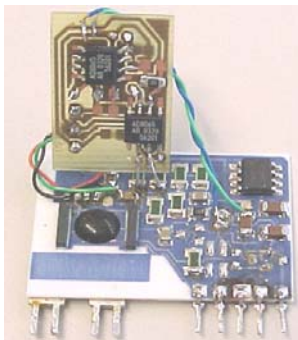


Fig.9: Modified AMR current sensor with two op-amp stages in series (MR-Sensor 2). The first op-amp stage is operating in open-loop mode, and the second op-amp stage is operating as an inverting amplifier with a gain of 8.5dB.

## V. CONCLUSION

AMR materials have the capability to measure currents with frequencies up to 1MHz, however commercial current sensors are limited to 100kHz. This paper has presented modifications that allow extending the frequency limit. It was shown how the frequency performance of the sensor element can be fully utilized. The frequency bandwidth of the proposed sensor is about 1MHz, which was verified by experimental measurement.

A disadvantage of AMR devices is the large temperature dependency, but can be eliminated through the use of a Wheatstone bridge arrangement of four sensing devices. The remaining offset due to manufacturing tolerances and the offset voltage and offset voltage drift of the op-amp stage can be eliminated to a large extent by a compensation network. The resistance of the compensation network resistors has to be laser trimmed. The remaining temperature drift of the sensor output signal is less than 1% of the nominal output signal range. It has been shown that the sensor has a low susceptibility if subjected to high  $dv/dt$  rates of the primary conductor.

An integration of the sensor's interface electronics into an ASIC would allow a reduction of the current sensor size. Therefore, the

sensor is highly attractive for integration into Intelligent Power Electronic Modules (IPEMs). The temperature dependency of the AMR devices there could be utilized for temperature measurement which would provide the basis for an on-line calculation and monitoring of the junction temperature of the IPEM power semiconductors.

## ACKNOWLEDGEMENT

This work was supported by the SENSiTEC GmbH which provided the Power Electronic Systems Laboratory with AMR sensor devices.

## REFERENCES

- [1] H. Lemme, "Ein Modul für alle Strombereiche – Magnetoresistive Stromsensoren kompakt wie noch nie, (in German)," Elektronik, (www.elektronik.de), Sept. 1999.
- [2] A.P. Friedrich and J. Kunze, "Universal Magnetoresistive Current Sensor for Automotive Applications," Publication by SENSiTEC GmbH, Im Amtmann 6, 6330 Wetzlar-Blankenfeld, Germany.
- [3] B. Drafts, F. W. Bell, "New Magnetoresistive Current Sensor Improves Power Electronic Performance," sensors online, (www.sensorsmag.com), Sept. 1999.
- [4] Ch. Xiao, L. Zhao, T. Asada, W.G. Odendaal and J.D. van Wyk, "An Overview of Integratable Current Sensor Technologies," Conference Record of the 38<sup>th</sup> IEEE IAS Annual Meeting, vol. 2, pp. 1251 - 1258, 12-16 Oct 2003.
- [5] F. Dettmann and U. Loreit, "Grundlagen Magnetoresistiver Sensoren," Institut für Mikrostrukturtechnologie und Optoelektronik (in German), SENSiTEC GmbH, Im Amtmann 6, 6330 Wetzlar-Blankenfeld, Germany (1998).
- [6] E.R. Olson, R.D. Lorenz, "Integrating Giant Magnetoresistive Current and Thermal Sensors in Power Electronic Moduls," 18<sup>th</sup> IEEE Applied Power Electronics Conference, Feb. 9-13, vol. 2, pp. 773-777 (2003).
- [7] Texas Instruments, TLE2037 datasheet, <http://focus.ti.com/docs/prod/folders/print/tle2037.html>.

